Journal of Fluids and Structures (2001) **15,** 39–57
doi:10.1006/jfls.2000.0326, available online at http://www.idealibrary.com on IDEAL®

ESTIMATION OF NONCONSERVATIVE AERODYNAMIC PRESSURE LEADING TO FLUTTER OF SPINNING DISKS

M. H. Hansen

Department of Solid Mechanics, Technical University of Denmark DK-2800 Lyngby, Denmark

A. Raman

School of Mechanical Engineering, Purdue University, West Lafayette, IN 47907, U.S.A.

AND

C. D. Mote Jr

Glenn L. Martin Institute, University of Maryland College Park, MD 207442, U.S.A.

(Received 11 February 1999, and in final form 25 May 2000)

An experimental method for predicting the onset of flutter of a disk spinning in a fluid medium is proposed. The method is based on a description of the aerodynamic loading on the disk as a distributed viscous damping force rotating relative to the disk. This model can arise from two aeroelastic theories described herein. It is shown analytically and experimentally that the few parameters of this model may be extracted from frequency response functions of the spinning disk. Parameters for a steel disk in air (with a near vacuum experiment as reference) are estimated at increasing rotation speeds below the onset of flutter. The flutter speed and mode of the disk are predicted. © 2001 Academic Press

1. INTRODUCTION

Current designs of disk saws and computer disk memory storage devices tend towards the use of thinner and higher speed disks. However, the aerodynamically induced instability of such devices poses a limit to their optimal design. Decreased disk thickness reduces the bending stiffness and thereby the critical rotation speed of the disk. Higher operating speeds increase the forces on the disk due to the aeroelastic coupling of the swirling flow and disk vibration. At a sufficiently high speed, the fluid–structure coupling leads to flutter instability of the disk where the response is dominated by a single backward traveling wave of an asymmetric vibration mode (D'Angelo & Mote 1993a; Renshaw *et al.* 1994). For this reason, the fluid–disk coupled problem controls the design of these high speed rotating disk devices. The aim of this work is to provide an experimental method for predicting the onset of flutter of spinning disks coupled to a surrounding fluid.

The stability of a flexible disk spinning very close to a rigid wall has been investigated by Hosaka & Crandall (1992), Huang & Mote (1995), Renshaw (1998) and others. These analyses depend on the Reynolds number of the fluid in the gap between the disk and wall being very small, so that classical hydrodynamic lubrication theory can be applied to model the pressure in the film. The coupling of the pressure to the disk motion is accomplished through the boundary conditions at the fluid–disk interface. These analyses

0889–9746/01/010039 + 19 $35.00/0 © 2001 Academic Press

have predicted successfully the flutter speeds and described the mechanisms through which the thin viscous flow in the gap couples to the disk. One of these mechanisms is referred to as *rotating damping*. Part of the aerodynamic pressure on the disk can be described as a distributed viscous damping force that rotates with respect to the disk. Hosaka & Crandall (1992) illustrated how a backward traveling wave is excited if the speed of this damping force becomes larger than the speed of a wave mode of the free disk.

The literature on the stability of a spinning disk coupled to flows in an unbounded fluid or bounded flows with nonsmall gapwidths has been relatively sparse. This is, in large part, due to the complexity of the swirling flow over the disk. D'Angelo & Mote (1993*a*) and Renshaw *et al.* (1994) experimentally and analytically investigated the stability of a disk spinning in an infinite medium. They modeled the fluid as a compressible, inviscid medium. Potential flow aerodynamics with the solution of the wave equation using Hankel transforms was then used to predict the fluid pressure generated on the disk surface as a function of the disk vibration. While this model qualitatively predicted the variation of flutter speeds with fluid density and the flutter mode correctly, no quantitative substantiation of the theory with respect to experimental flutter speeds was found.

Yasuda *et al.* (1992) proposed that the aerodynamic force on a disk spinning in an infinite medium can be written in terms of "lift" and "damping" forces. This representation of the aerodynamic pressure is a special case of a distributed rotating damping force. They assumed that the ratio between the lift and damping force, which is equivalent to the speed of the damping force, was proportional to the rotation speed. Similar to the analysis for disks spinning close to a wall, they showed that flutter of a single backward traveling wave could arise at a particular rotation speed. However, no physical basis for the use of the rotating damping model in an infinite fluid medium was provided, and no prescription (experimental or otherwise) was suggested to obtain the proportionality constant between the speed of the disk and the damping force.

In this paper, we suggest an experimental method for predicting flutter of a disk spinning in a fluid. The method is based on the rotating damping model where the relationship between the speed of the disk and the damping force is obtained experimentally. First, a physical basis for the rotating damping model is discussed on the basis of both inviscid and viscous flow theory. Then we show how the speed of the damping force can be extracted from measurements of the frequency response of the spinning disk. The extraction is based on the experimental observations that forward traveling waves are more damped than backward traveling waves, which was first observed by Campbell (1924) and later noted by Tobias & Arnold (1957). Two experiments are presented for a steel disk, one spinning in near vacuum and then spinning in air at ambient pressure. In the absence of air, no difference between the damping of the pairs of forward and backward traveling wave pairs is observed. In the presence of air, the observations by Campbell (1924) and Tobias & Arnold (1957) are confirmed. By measuring the frequency response at increasing rotation speeds, we obtain an experimental relationship between the speed of the disk and the damping force. It is nonlinear and mode-dependent. The flutter speed and mode of the disk are predicted by extrapolation of this relationship.

2. THEORETICAL MODEL

2.1. Equations of Motion

Consider the schematic of the system and the definition of coordinate systems in Figure 1. An annular disk of thickness h is clamped at radius a and is free at the outer radius b. It is rotating with the constant angular speed Ω^* (here and subsequently, the asterisk denotes

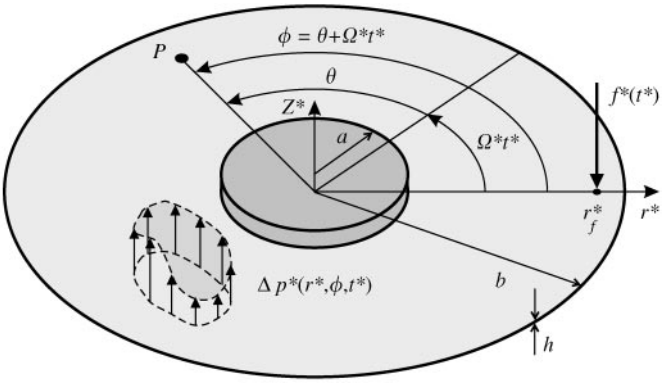

Figure 1. Schematic of spinning disk system and definition of coordinate systems.

a dimensional quantity). The disk is thin ($h \ll b$) and isotropic with Young's modulus E, Poisson's ratio ν, and density ρ. Two cylindrical coordinate systems are used interchangeably when describing the transverse displacement w^* of a material point P on the disk: A *ground-fixed frame* (r^*, φ, z^*) and a *co-rotating disk fixed frame* (r^*, θ, z^*), where $\varphi = \theta + \Omega^* t^*$. A stationary external force $f^*(t^*)$ acts transversly at point (r_f^*, φ_f) at $\varphi_f \equiv 0$. The aerodynamic loading on the disk, described by the pressure difference across the upper and lower surfaces, is Δp^*.

The linear field equation governing small transverse motions of a thin spinning disk is given by the linearized Kirchhoff plate theory and can be found in several papers [e.g. Hosaka & Crandall (1992); Renshaw (1998)]. With introduction of the nondimensional variables

$$w = \frac{w^*}{h}, \quad r = \frac{r^*}{b}, \quad \kappa = \frac{a}{b}, \quad t = \frac{t^*}{t_0}, \quad \Omega = \Omega^* t_0, \quad \Delta p = \frac{\Delta p^* t_0^2}{\rho h^2}, \quad f = \frac{f^* t_0^2}{h^2 b^2 \rho}, \tag{1}$$

where $t_0 = \sqrt{12(1-\nu^2)\rho b^4/(Eh^2)}$ is a characteristic time-constant, the governing field equation in the ground-fixed frame becomes

$$w_{,tt} + 2\Omega w_{,t\varphi} + \Omega^2 w_{,\varphi\varphi} + \mathrm{D}[w_{,t}] + \mathrm{K}[w] = \Delta p + \frac{1}{r}\,\delta(r - r_f)\delta(\varphi) f(t), \tag{2}$$

where

$$\mathrm{K}[w] = \nabla^4 w - \frac{1}{r}(r\sigma_{rr} w_{,r})_{,r} - \frac{1}{r^2}\,\sigma_{\varphi\varphi} w_{,\varphi\varphi} \tag{3}$$

is a stiffness operator including membrane stress effects, D is a spatial operator modeling the structural dissipation, and δ is Dirac's delta function. Note that the shear stress due to fluid drag on the surfaces of the disk is neglected. The axisymmetrical membrane stresses due to the rotation of the disk can be written in the form $\sigma_{rr} = \sigma_{rr}^r(r, \kappa, \nu)\Omega^2$ and $\sigma_{\varphi\varphi} = \sigma_{\varphi\varphi}^r(r, \kappa, \nu)\Omega^2$. The radial functions σ_{rr}^r and $\sigma_{\varphi\varphi}^r$ can be derived from in-plane force equilibrium equations and in-plane boundary conditions (D'Angelo & Mote 1993*b*), like vanishing radial displacement at the clamping radius and vanishing radial normal stress at the free outer rim. The boundary conditions for the transverse displacement

of a clamped–free disk are

$$w|_{r=\kappa} = 0 \quad (w_{,rr} + v(w_{,\varphi\varphi} + w_{,r}))|_{r=1} = 0,$$
$$w_{,r}|_{r=\kappa} = 0 \quad [(\nabla^2 w)_{,r} + (1-v)(w_{,r} - w)_{,\varphi\varphi}]|_{r=1} = 0, \tag{4}$$

with an additional condition of circumferential periodicity $w(r, \varphi, t) = w(r, \varphi + 2\pi, t)$.

The stiffness operator K is self-adjoint with respect to the boundary conditions (4) and the periodicity condition. For a free–free viscoelastic disk, material damping may be modeled as proportional to the rate of the bending strains $\mathrm{D}[w_{,t}] = \nabla^4 w_{,t}$ (Hosaka & Crandall 1992), in which case D is self-adjoint and positive definite. The clamping of the disk will lead to frictional damping at the clamping interface. We assume that this dissipation can also be modeled by the term $\mathrm{D}[w_{,t}]$ where D is self-adjoint and positive definite. Hence, there is no structural coupling of modes and the structural damping is purely dissipative.

2.2. Aeroelastic Model

We consider a linear nonconservative aerodynamic pressure differential in the co-rotating frame of the following general form:

$$\Delta p(r, \theta, t) = -\mathrm{C}[(w_{,t} - \Omega_d w_{,\theta})], \tag{5}$$

where $\Delta p(r, \theta, t)$ represents the pressure differential across the surfaces of the disk generated by transverse motion. The linear spatial operator C is assumed to be self-adjoint and positive definite with respect to the boundary conditions (4). This general representation describes the pressure field as consisting of a dissipative form, $\mathrm{C}[w_{,t}]$ and a circulatory form $\mathrm{C}[\Omega_d w_{,\theta}]$.

The aeroelastic model (5) may also be interpreted as a distributed viscous damping force that rotates at the speed Ω_d relative to the disk (Hosaka & Crandall 1992). We can see this by defining $\varphi_d = \theta + \Omega_d t$ and transforming the pressure (5) into a coordinate system (r, φ_d, z). In this coordinate system, the pressure is described by single viscous damping term $-\mathrm{C}[w_{,t}]$, i.e., the damping force is "stationary" though the disk is rotating with the speed Ω_d. In the co-rotating disk fixed frame (r, θ, z), the damping force is rotating in the negative θ-direction with speed Ω_d, subsequently called the *damping speed*.

The representation of the pressure (5) includes, as a special case, the aeroelastic model of Yasuda *et al.* (1992). To recover their model, set $\mathrm{C} = C_D$ where C_D is a constant damping coefficient, and $\Omega_d = \Omega C_L / C_D$ where the constant C_L is referred to as a lift coefficient. We see that Yasuda *et al.* (1992) assume the damping speed to be proportional to the rotation speed. They provided no discussion of a physical basis for the rotating damping model. In the next two sections we describe two aeroelastic theories that motivate this model.

2.2.1. Piston theory

The piston theory models the interaction between a vibrating structure and a supersonic potential flow (Dowell 1975). At supersonic speeds, it can be shown that every point on a vibrating surface can be modeled as a piston vibrating in a tube that is fixed in the fluid coordinates and is independent of the surrounding tubes. The pressure arising on a piston vibrating with the velocity v is $-\sqrt{\rho_f B}\, v$, where B and ρ_f are the bulk compressibility and density of the fluid. Because potential flow models inviscous fluids, the flow over the spinning disk remains stationary. Thus, the velocity of a surface point on the disk is

$w^*_{,t^*}(r^*, \varphi, t^*)$ measured in fluid fixed coordinates. In the co-rotating frame the aerodynamic pressure therefore becomes

$$\Delta p(r, \theta, t) = -\sqrt{12(1-\nu^2)}\frac{b^2}{h^2}\sqrt{\frac{\rho_f B}{\rho E}}\,(w_{,t} - \Omega w_{,\theta}), \tag{6}$$

which describes a distributed damping force rotating with the speed Ω. Although the flow over a spinning disk is dominated by viscous effects and is seldom supersonic, the aerodynamic pressure (6) is one instance of a rotating damping model derived within aeroelasticity.

2.2.2. Viscous flow theory

The rotating damping model may also arise in models that include the viscosity of the surrounding fluid. The original example of the rotating damping model is the aerodynamic pressure on a disk spinning close to a rigid wall. The low Reynolds number of the fluid film between disk and wall yields that this aeroelastic model can be derived directly from the reduced Navier-Stokes equations of lubrication theory. Hosaka & Crandall (1992), Huang & Mote (1995) and others showed that the fluid damping speed in this case is $\Omega_d = \Omega/2$.

The Reynolds number for the swirling flow over a disk spinning close in an unbounded viscous fluid is high, and turbulent regions will often exist on the disk towards the outer rim (D'Angelo & Mote 1993*a*). Derivation of the aerodynamic pressure directly from Navier-Stokes equations is in this case difficult. However, it is possible that the rotating damping model of the aerodynamic pressure may still arise due to the boundary conditions for the disk-fluid interface, whether the fluid is enclosed, or unbounded. The transverse disturbance of the viscous flow near the disk is given by the terms $w_{,t}$, and $w_{,\theta}$ multiplied by some circumferential velocity of the flow. This disturbance is assumed to be of highest order the feedback through Navier-Stokes equations to the aerodynamic pressure on the disk, whereby a rotating damping type of model will arise. The speed of the damping force is affected by the circumferential velocity of flow near the disk which is directly related to the rotation speed of the disk. This relationship needs not to be linear as in the other examples of the rotating damping model. For further discussion of these considerations see Hansen (1999).

2.3. Aeroelastic Decoupling

In this section, we show that aeroelastic effects cause at most a weak inter-modal coupling, i.e., between modes with different number of nodal diameters and circles. A Galerkin projection, neglecting this weak coupling, leads to structurally and aerodynamically decoupled equations of motion of pairs governing forward and backward traveling waves.

With the pressure (5) transformed into ground-fixed coordinates (r, φ, z), the field equation becomes

$$w_{,tt} + 2\Omega w_{,t\varphi} + \Omega^2 w_{,\varphi\varphi} + \mathrm{K}[w] + \mathrm{D}[w_{,t}] + \mathrm{C}[w_{,t} + (\Omega - \Omega_d)w_{,\varphi}] = \frac{1}{r}\,\delta(r - r_f)\delta(\varphi)f(t). \tag{7}$$

Noting that $w(r, \varphi, t) = w(r, \varphi + 2\pi, t)$, we assume a solution in separable form (Hosaka & Crandall 1992)

$$w(r, \varphi, t) = W_{mn}(r, \varphi)\mathrm{e}^{\lambda t} \tag{8}$$

with

$$W_{mn}(r, \varphi) = R_{mn}(r)\mathrm{e}^{\mathrm{i}n\varphi}, \tag{9}$$

where the radial functions are complex $R_{mn}(r) = R^R_{mn}(r) + \mathrm{i}R^I_{mn}(r)$. The indices m and n describe the numbers of nodal circles and diameters of the mode. Substituting equation (9) into equation (7) with $f \equiv 0$, we get

$$(\lambda^2 + \mathrm{i}2\lambda n\Omega - n^2\Omega^2)R_{mn} + \mathrm{K}^r_n[R_{mn}] + \lambda \mathrm{D}^r_n[R_{mn}] + (\lambda + \mathrm{i}n(\Omega - \Omega_d))\mathrm{C}^r_n[R_{mn}] = 0, \tag{10}$$

where the radial stiffness operator becomes

$$\mathrm{K}^r_n[R_{mn}] = \left((\,)_{,rr} + \frac{1}{r}(\,)_{,r} - \frac{n^2}{r^2} \right)^2 R_{mn} - \frac{1}{r}(r\sigma_{rr}R_{mn,r})_{,r} + \frac{n^2}{r^2}\sigma_{\varphi\varphi}R_{mn}, \tag{11}$$

and D^r_n and C^r_n are radial operators arising from substitution of equation (8) into the self-adjoint operators D and C.

The characteristic equation (10) represents the nonself-adjoint eigenvalue problem associated with equation (7). Note that the radial component of the eigenfunction $R_{mn}(r)$ must be complex valued for the mode shapes represented by equaiton (9) to possess curved nodal lines (Hosaka & Crandall 1992).

The nonself-adjoint eigenvalue problem with its associated characteristic equation (10), does not in general possess orthogonal eigenfunctions. However, owing to the separable form of the eigenfunctions (9), a restricted orthogonality can be shown. Let the domain be $\mathscr{D} = \{(r, \varphi) : \kappa \le r \le 1, 0 \le \varphi < 2\pi\}$, and denote the space of complex-valued functions on $\mathscr{D}$ as $(\mathbb{C}, \mathscr{D})$. Define an inner product on $(\mathbb{C}, \mathscr{D})$ as follows:

$$\langle u, v \rangle = \int_0^{2\pi} \int_\kappa^1 u\,\bar{v} r \,\mathrm{d}r \,\mathrm{d}\theta\,, \quad \forall u, v \in (\mathbb{C}, \mathscr{D}), \tag{12}$$

where the overbar represents a complex conjugate. Consider the subset $L_2(\mathbb{C}, \mathscr{D})$ of complex-valued functions with finite L_2-norm on D. Then, we must have $W_{mn}(r, \varphi) \in L_2(\mathbb{C}, \mathscr{D})$. Under the inner product (12), the following restricted orthogonality exists in the aeroelastic eigenvalue problem corresponding to equation (10):

$$\langle W_{m_1 n_1}, W_{m_2 n_2} \rangle = 0 \quad \text{if } n_1 \ne n_2; \tag{13}$$

however, $\langle W_{m_1 n_1}, W_{m_2 n_2} \rangle \ne 0$ in general for $m_1 \ne m_2$. This shows that modes possessing the same nodal diameter number can be aeroelastically coupled, whereas the orthogonality of the circumferential mode shapes (9) ensures decoupling of modes with different nodal diameter numbers. Because $\langle W_{m_1 n_1}, W_{m_2 n_2} \rangle = 0$ for $m_1 \ne m_2$ for a stationary disk and at the flutter speed [cf. Hosaka & Crandall (1992)], we assume that the effect of the curvature of nodal lines to be small, so that $\langle W_{m_1 n_1}, W_{m_2 n_2} \rangle = \mathcal{O}(\varepsilon)$ for $m_1 \ne m_2$ at pre-flutter rotation speeds ($\varepsilon \ll 1$).

A Galerkin projection of equation (7) onto the eigenfunction space based on modes without nodal circles ($m = 0$), will therefore truncate aeroelastic coupling terms of order $\mathcal{O}(\varepsilon)$ only. This truncation is assumed to be valid when the order of the error is compared to the experimental error. It allows use of a modal expansion in terms of these lower asymmetrical modes

$$w(r, \varphi, t) \approx \sum_{n=1}^{N} R_{0n}(r)[z_{0n}(t)\mathrm{e}^{\mathrm{i}n\varphi} + \bar{z}_{0n}(t)\mathrm{e}^{-\mathrm{i}n\varphi}], \tag{14}$$

where $z_{0n}(t)$ are the complex *wave coordinates* (Lee & Kim 1995) of mode $(0, n)$. Substituting equation (14) into equation (7), taking the inner products with $R_{0k}(r)e^{ik\varphi}$, and using the orthogonality (13), we obtain N decoupled equations of motion, to the leading order

$$\ddot{z}_{0n} + i2n\Omega\dot{z}_{0n} - n^2\Omega^2 z_{0n} + \tilde{\omega}_{0n}^2 z_{0n} + c_{0n}[\dot{z}_{0n} + in(\Omega - \Omega'_{d_{0n}})z_{0n}] = R_{0n}(r_f)f(t), \quad (15)$$

where the complex conjugate equations are omitted, and we define $\langle W_{0n}, W_{0n}\rangle \equiv 1$. The stiffness due to bending and centrifugal stresses is given by $\tilde{\omega}_{0n}^2 = \langle W_{0n}, K[W_{0n}]\rangle$. We see that $\tilde{\omega}_{0n}$ is the *natural frequency* of the mode $(0, n)$ in the co-rotating frame, which can be related to the rotation speed through the approximation [e.g., Campbell (1924), D'Angelo & Mote (1993b)]

$$\tilde{\omega}_{0n} \approx \sqrt{\omega_{0n}^{st^2} + s_{0n}\Omega^2}, \quad (16)$$

where ω_{0n}^{st} is the natural frequency of the stationary disk and s_{0n} is a centrifugal stiffening coefficient.

A single damping coefficient $c_{0n} = \langle W_{0n}, D[W_{0n}]\rangle + \langle W_{0n}, C[W_{0n}]\rangle$ describes the magnitude of both structural and fluid damping forces. The damping speed is $\Omega'_{d_{0n}} = \Omega_{d_{0n}}\langle W_{0n}, C[W_{0n}]\rangle / (\langle W_{0n}, D[W_{0n}]\rangle + \langle W_{0n}, C[W_{0n}]\rangle)$, where $\Omega_{d_{0n}}$ is actual speed of the fluid damping force defined by equation (5). Because operators C and D are positive definite, this damping speed is less than the actual speed.

The modal expansion (14) and the decoupled equations of motion (15) are assumed to describe the response under aerodynamic pressure and excitation force.

3. EXTRACTION OF MODEL PARAMETERS FROM FREQUENCY RESPONSES

Prediction of the onset of flutter of the spinning disk requires determination of the model parameters $\tilde{\omega}_{0n}$, c_{0n} and $\Omega'_{d_{0n}}$ as functions of rotation speed.

3.1. Wave Poles of the Aerodynamically Loaded Disk

The response of the disk is approximated by the modal expansion (14) and the wave coordinates $z_{0n}(t)$ are determined from the equation of motion (15). We assume a solution of the form $z_{0n}(t) = Z_{0n}(\omega)e^{i\omega t}$, where $Z_{0n}(\omega)$ is the frequency response described in wave coordinates. Substitution of this solution into equation (14) yields

$$w(r, \varphi, t) \approx \sum_{n=1}^{N} R_{0n}(r)[Z_{0n}(\omega)e^{i(\omega t + n\varphi)} + \bar{Z}_{0n}(\omega)e^{-i(\omega t + n\varphi)}]. \quad (17)$$

The exponent $\omega t + n\varphi$ shows that equation (17) describes modal waves traveling around the disk with speed $-\omega/n$ relative to the ground fixed frame. Each asymmetrical mode $(0, n)$ is separated into pairs of waves traveling in both directions on the disk. For a pole of $Z_{0n}(\omega)$ in the negative part of the frequency domain ($\omega < 0$), the modal response is a *forward traveling wave* (FTW). For a pole in the positive frequency domain ($\omega > 0$), the response is a *backward traveling wave* (BTW).

These *wave poles* of mode $(0, n)$ are determined from the characteristic equation obtained by inserting a solution of the form $z_{0n}(t) = e^{\lambda_{0n}t}$ into equation (15) with $f \equiv 0$. The complex pole $\lambda_{0n} = \alpha_{0n} + i\omega_{0n}$ determines the *wave frequency* of the resonance response, ω_{0n}, and the stability of the plane equilibrium of the disk through the *damping factor* of the wave, α_{0n}. In the ground fixed frame, the characteristic equation becomes

$$(\lambda_{0n} + in\Omega)^2 + \tilde{\omega}_{0n}^2 + c_{0n}(\lambda_{0n} + in\Omega - in\Omega'_{d_{0n}}) = 0. \quad (18)$$

Note that the poles can be defined in the co-rotating frame as $\hat{\lambda}_{0n} = \lambda_{0n} + \mathrm{i}n\Omega$. To realize this shift in wave frequency $\hat{\omega}_{0n} = \omega_{0n} + n\Omega$ between the two coordinate systems, one can insert the transformation $\varphi = \theta + \Omega t$ into equation (17).

We introduce a damping ratio and a normalized damping speed:

$$\hat{c}_{0n} = \frac{c_{0n}}{\tilde{\omega}_{0n}} \quad \text{and} \quad \hat{\Omega}'_{d,mn} = \frac{n\Omega'_{d_{0n}}}{\tilde{\omega}_{0n}}, \tag{19}$$

where the quantity $\hat{\Omega}'_{d_{0n}}$ is the ratio between the damping speed and wave speed of the FTW and BTW in the co-rotating frame. Yasuda *et al.* (1992) showed that flutter occurs when $\hat{\Omega}'_{d_{0n}} = 1$, thus $\hat{\Omega}'_{d_{0n}}$ is $\mathcal{O}(1)$. With the parameters (19) the characteristic equations for the poles in the co-rotating frame become

$$\hat{\lambda}_{0n}^2 + \tilde{\omega}_{0n}^2 + \tilde{\omega}_{0n}\hat{c}_{0n}(\hat{\lambda}_{0n} - \mathrm{i}\tilde{\omega}_{0n}\hat{\Omega}'_{d_{0n}}) = 0 \tag{20}$$

with solutions

$$\hat{\lambda}_{0n} = \tilde{\omega}_{0n}\left(-\frac{\hat{c}_{0n}}{2} \pm \sqrt{\left(\frac{\hat{c}_{0n}}{2}\right)^2 - (1 - \mathrm{i}\hat{c}_{0n}\hat{\Omega}'_{d_{0n}})}\right). \tag{21}$$

With light damping $\hat{c}_{0n} \ll 1$, for example for a steel disk in air, the first term under the square root can be neglected. Taylor expansion about $\hat{c}_{0n}\hat{\Omega}'_{d_{0n}} = 0$ gives the approximate wave poles in the ground-fixed frame

$$\lambda_{0n}^F \approx -\frac{c_{0n}}{2}\left(1 + \frac{n\Omega'_{d_{0n}}}{\tilde{\omega}_{0n}}\right) - \mathrm{i}(\tilde{\omega}_{0n} + n\Omega) \quad \text{and} \quad \lambda_{0n}^B \approx -\frac{c_{0n}}{2}\left(1 - \frac{n\Omega'_{d_{0n}}}{\tilde{\omega}_{0n}}\right) + \mathrm{i}(\tilde{\omega}_{0n} - n\Omega), \tag{22}$$

where the superscripts F and B refer to the direction of the corresponding wave given by the sign of the wave frequency. Note that the frequency of the BTW of mode $(0, n)$ vanishes at $\Omega_{0n}^c = \tilde{\omega}_{0n}(\Omega_{0n}^c)/n$. The speed Ω_{0n}^c is called the *critical rotation speed* of mode $(0, n)$.

From the damping factors of the poles (22), we see that FTWs are more damped than BTWs when $\Omega'_{d_{0n}} > 0$. As shown by Yasuda *et al.* (1992), the flutter of a BTW can occur when the damping speed $\Omega'_{d_{0n}}$ equals the wave speed of the BTW, $\tilde{\omega}_{0n}/n$. Both speeds are functions of the rotation speed Ω. The smallest rotation speed, denoted Ω_f where $\Omega'_{d_{0n}}(\Omega_f) = \tilde{\omega}_{0n}(\Omega_f)/n$, is called the *flutter speed* and mode $(0, n)$ is the *flutter mode*.

3.2. Frequency Response of the Aerodynamically Loaded Disk

Let the displacement response of the aerodynamically loaded disk under the excitation $f(t)$ at $(r_f, 0)$ be measured at (r_x, φ_x). This response is approximated by the modal expansion (14), which in the frequency domain can be written as

$$W(\omega) = \int_{-\infty}^{\infty} w(r_x, \varphi_x, t)\, \mathrm{e}^{-\mathrm{i}\omega t}\, \mathrm{d}t \approx \sum_{n=1}^{N} R_{0n}(r_x)[Z_{0n}(\omega)\mathrm{e}^{\mathrm{i}n\varphi_x} + Z'_{0n}(\omega)\mathrm{e}^{-\mathrm{i}n\varphi_x}], \tag{23}$$

where $Z_{0n}(\omega)$ and $Z'_{0n}(\omega)$ are the Fourier transforms of the complex wave coordinate $z_{0n}(t)$ and its complex conjugate $\bar{z}_{0n}(t)$. These relate to the excitation $f(t)$ through the Fourier transform of the equation of motion (15) and its complex conjugate

$$Z_{0n}(\omega) = H_{0n}^{zf}(\omega)R_{0n}(r_f)F(\omega) \quad \text{and} \quad Z'_{0n}(\omega) = H_{0n}^{\bar{z}\bar{f}}(\omega)R_{0n}(r_f)F(\omega), \tag{24}$$

where the transfer function $H_{0n}^{zf}(\omega)$ and $H_{0n}^{\bar{zf}}$ are

$$H_{0n}^{zf}(\omega) = \frac{1}{\tilde{\omega}_{0n}^2 - (\omega + n\Omega)^2 + \mathrm{i}c_{0n}(\omega + n\Omega - n\Omega'_{d_{0n}})} \tag{25}$$

and $H_{0n}^{\bar{zf}}(\omega) = \overline{H_{0n}^{zf}}(-\omega)$ (Lee & Kim 1995). Note that in the second of equation (24), we have utilized the real property of $f(t)$.

The frequency response function (FRF) is defined as $W(\omega)/F(\omega)$. Thus from equations (23) and (24), the FRF of the aerodynamically loaded disk is

$$H(\omega) = \frac{W(\omega)}{F(\omega)} \approx \sum_{n=1}^{N} R_{0n}(r_f)R_{0n}(r_x)[H_{0n}^{zf}(\omega)\mathrm{e}^{\mathrm{i}n\varphi_x} + \overline{H_{0n}^{zf}}(-\omega)e^{-\mathrm{i}n\varphi_x}]. \tag{26}$$

3.2.1. Extraction of model parameters

Because the transfer function $\overline{H_{0n}^{zf}}$ has the complex conjugate poles of H_{0n}^{zf}, see equation (25), the wave poles of the FTWs are reflected from the negative into the positive half-plane of the frequency domain, through the term $\overline{H_{0n}^{zf}}(-\omega)$ in equation (26). The wave frequencies of the FTWs and BTWs, given by equation (22), may be approximated by

$$\omega_{0n}^F \approx \tilde{\omega}_{0n} + n\Omega \quad \text{and} \quad \omega_{0n}^B \approx \tilde{\omega}_{0n} - n\Omega \tag{27}$$

for subcritical rotation speeds $\Omega < \Omega_{0n}^c$ (when the speed is supercritical, the wave frequency of the BTW is $-\tilde{\omega}_{0n} + n\Omega$). Note that the damping factors of the poles are not affected by the reflection.

Now assume that we have estimated the wave poles of the FTW and BTW as $\alpha_{0n}^F + \mathrm{i}\omega_{0n}^F$ and $\alpha_{0n}^B + \mathrm{i}\omega_{0n}^B$. From the relations (27), we can obtain two estimates for the natural frequency $\tilde{\omega}_{0n}$ from the wave frequencies ω_{0n}^F and ω_{0n}^B. The other two model parameters c_{0n} and $\Omega'_{d_{0n}}$ can be extracted from the damping factors α_{0n}^F and α_{0n}^B. Algebraic manipulation of the wave poles (22) gives

$$c_{0n} \approx \alpha_{0n}^F + \alpha_{0n}^B \quad \text{and} \quad c_{0n}\Omega'_{d_{0n}} \approx \frac{\tilde{\omega}_{0n}}{n}(\alpha_{0n}^F - \alpha_{0n}^B), \tag{28}$$

where it is noted that the damping speed $\Omega'_{d_{0n}}$ is not isolated. The estimated damping factors are normally small and subject to error. To avoid the inherent error in the division of $c_{0n}\Omega'_{d_{0n}}$ by $\alpha_{0n}^F + \alpha_{0n}^B$, we will instead estimate the damping coefficient c_{0n} and the product $c_{0n}\Omega'_{d_{0n}}$ by experiment.

3.2.2. Identification of waves

To identify the waves in the experimental FRF, two displacement responses must be recorded at two ground fixed positions (r_{x_1}, φ_{x_1}) and (r_{x_2}, φ_{x_2}). The wave number n and direction may then be extracted from the phase of the complex cross-spectrum between these responses when evaluated at the wave frequencies. The single-mode cross-spectrum between $W_{0n}^{x_1}$ and $W_{0n}^{x_2}$ from equations (23) and (24) is

$$W_{0n}^{x_1}\overline{W_{0n}^{x_2}} = R_{0n}(r_{x_1})R_{0n}(r_{x_2})R_{0n}(r_f)^2|F|^2[|H_{0n}^{zf}(\omega)|^2\mathrm{e}^{\mathrm{i}n(\varphi_{x_1}-\varphi_{x_2})} + |H_{0n}^{zf}(-\omega)|^2\mathrm{e}^{-\mathrm{i}n(\varphi_{x_1}-\varphi_{x_2})}$$
$$+ H_{0n}^{zf}(\omega)H_{0n}^{zf}(-\omega)\mathrm{e}^{\mathrm{i}n(\varphi_{x_1}-\varphi_{x_2})} + \overline{H_{0n}^{zf}(\omega)H_{0n}^{zf}(-\omega)}\mathrm{e}^{-\mathrm{i}n(\varphi_{x_1}-\varphi_{x_2})}]. \tag{29}$$

At the wave frequency of the FTW where $|H_{mn}^{zf}(-\omega)|^2 \gg |H_{mn}^{zf}(\omega)|^2$ the phase of (28) is $-n(\varphi_{x_1} - \varphi_{x_2})$. Similarly, the phase is $n(\varphi_{x_1} - \varphi_{x_2})$ at the wave frequency of the BTW. The wave number n and direction of a wave is therefore easily obtained from the known angle $\varphi_{x_1} - \varphi_{x_2}$ and the sign of the phase. For further details on mode identification of spinning disks see Ahn & Mote (1998).

4. EXPERIMENTS

Two experiments are performed with a steel disk. In the first, the disk is spinning in near vacuum (about 1% of the standard atmospheric pressure). It serves as a reference for another experiment where the disk is spinning in air at ambient pressure. The purpose of this experiment is to illustrate the method for predicting the flutter speed of the disk which has been suggested in the previous section.

4.1. Set-up and Experimental Procedure

The apparatus was used in D'Angelo & Mote (1993*a*) and it was built especially for accurate measurement of vibration of high-speed disks. The design minimizes sources of experimental error including bearing noise, rotor unbalance, and thermal stresses due to heating at the bearings. The motor and spindle are housed in a vacuum chamber with the ambient pressure adjustable down to $\sim$1 mmHg. Primary elements of the apparatus include a thin disk with thick clamping collars, a high-precision spindle, and vibration measurement instrumentation.

Experiments are performed on a plate of nominal outer diameter 356 mm, and the clamping diameter is 106·7 mm resulting in a clamping ratio of 0·3. The material of the disk is 8660 steel, hardened to 42 HRC, then ground to a thickness of 0·775 mm with maximum runout less than 0·10 mm. Residual stresses from manufacture are relieved after grinding, creating a disk that is nearly stress-free. The precision spindle is directly motorized and can spin the disk and collar assembly in the range 300–14 400 rpm.

The experimental configuration is shown in Figure 2. A dual electromagnetic actuator located at a radius of 160 mm excites the disk with the signal from the signal generator. Two inductance-type displacement transducers measure the transverse motion of the plate at a radial distance of 148 mm. They have an angular separation of 18° and a linear range of 2·5 mm with a resolution of 0·20 μm. The vibration response from the two displacement probes and the input signal to the electromagnets are input to a Tektronix 2630MS spectrum analyzer. A counter connected to an optical probe measures the rotation speed with a precision of 0·1 Hz.

4.1.1. Obtaining the frequency response functions

The disk is excited ramdomly by the electromagnets in frequency bands of interest. The response is sampled 2048 times by the two displacement probes. To increase the frequency resolution, the FRF at each rotation speed is divided into 100 Hz frequency bands with 25 Hz of overlap, starting from 0, 75, 150 Hz, etc. Therefore, the frequency resolution is 100/1024 Hz, or approximately 0·1 Hz.

The force generated by the electromagnetic coils, $f(t)$, cannot be measured in the present set-up. Instead, the voltage across the coils $v(t)$ is recorded and used in the computation of the FRF. Ellis & Mote (1979) discussed the requirements for the operation of a dual electromagnet set-up to ensure a linear voltage–force relationship, $F(\omega) \propto V(\omega)$. The driving frequency must be well below the cut-off frequency of the coil-circuit, the spacing between

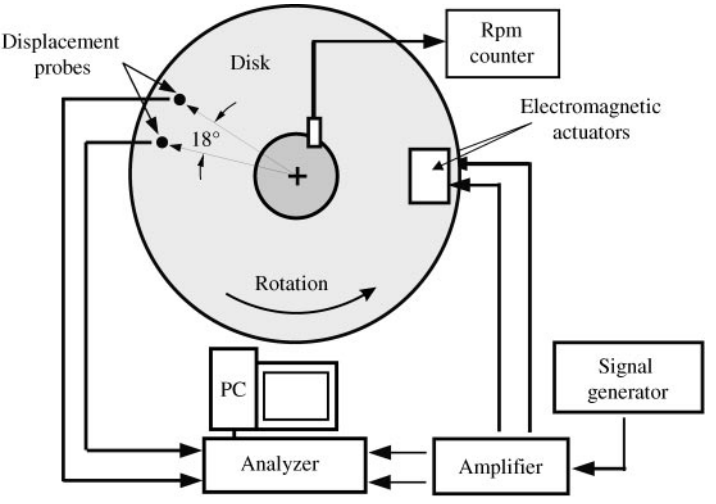

Figure 2. Schematic of the set-up.

the magnets must be large compared to the disk vibration, and the amplitude of the current variations must be small compared to the steady current. All these requirements are considered in the experiments.

4.1.2. Estimation of natural frequencies and damping factors

After all FRFs are recorded, they are processed on the PC with modal analysis software STAR [SMS 1990] to obtain wave frequencies and damping factors for the waves of the four lowest asymmetrical modes ($m = 0$ and $n = 1, 2, 3, 4$) from *Rational Fraction Polynomial* fits. Because two displacement probes are used, each wave frequency and damping factor represents an average of two estimations, which in the case of the overlap of the FRFs becomes an average of four estimations.

As shown in Section 3.2.1, the natural frequencies of the modes in the co-rotating frame can be estimated from the wave frequencies of the corresponding FTW and BTW through relations (27). Two estimates of the natural frequency $\tilde{\omega}^*_{0n}$ of mode $(0, n)$ are therefore obtained from the wave frequencies of the corresponding wave pairs, the rotation speed Ω^* and the wave number n. Because the accuracy of the rotation speed and the frequency resolution are both 0·1 Hz, the measurement error of the natural frequencies is estimated to be $0{\cdot}1(1 + n)$ Hz. The measurement error of the damping factors is estimated from test of the disk spinning in vacuum.

4.2. Results

In the experiments the natural frequencies of the four modes and the damping factors for the corresponding waves are estimated at increasing rotation speeds. We present first the results of the reference experiment where aerodynamic loading can be neglected. The results of the experiment with the disk spinning in air at ambient pressure are then presented. From the results of this experiment, the model parameters are estimated as function of the rotation speed at pre-flutter speeds and used to predict the flutter speed of the disk at ambient pressure.

4.2.1. Reference experiment in vacuum

The pressure in the chamber is maintained in the range 5–10 mmHg. Natural frequencies and damping factors of the four wave pairs are estimated at 17 rotation speeds in range 0–48 Hz at 3 Hz intervals.

In Figure 3 the estimated natural frequencies of each wave are displayed versus rotation speed. The difference between the frequency of a FTW and the corresponding BTW is less than 0·5%, and below the measurement error of $0{\cdot}1(1 + n)$ Hz for all modes and at all rotation speeds. The curves in Figure 3 are nonlinear least square fits based on the theoretical relation (15). The result of the curve fits is listed in Table 1. The correlation coefficients show that (15) is a good approximation to the relation between the natural frequency and the rotation speed.

The critical speeds of the four modes are also listed in Table 1. Note that mode (0, 1) has no critical speed as it has been proven by Renshaw & Mote (1992) .

In Figure 4 the estimated damping factors of the FTWs and BTWs are displayed versus rotation speed. The damping factors of a FTW and the corresponding BTW interchange magnitude at least five times during the 17 measurements, i.e., no systematic difference in damping between the FTW and BTW can be observed. Furthermore, the damping factors

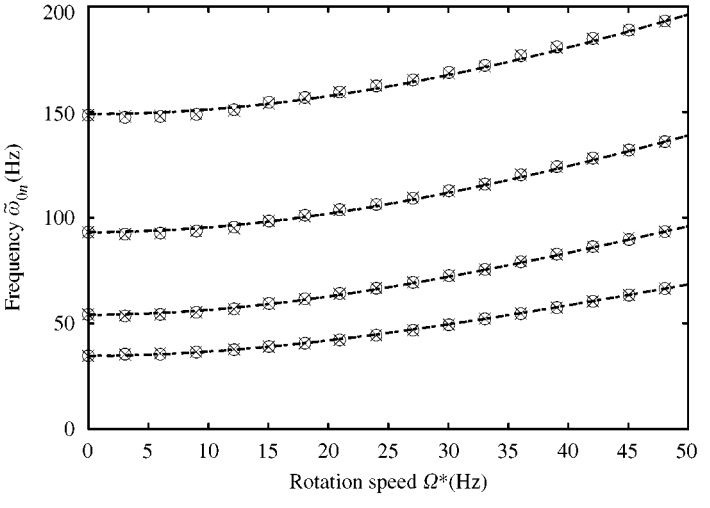

Figure 3. Natural frequencies calculated using relations (27) based on wave frequencies of BTWs ($\times$) and FTWs ($\odot$) measured at low pressure. The curve fits are based on equation (16).

TABLE 1
Natural frequencies of the stationary disk ω_{0n}^{st*}, centrifugal stiffening coefficients s_{0n}, and critical speeds Ω_{0n}^{c*} at low pressure

Wave	ω_{0n}^{st*} (Hz)	s_{0n}	Correlation	Critical speed (Hz)
1B	34·70	1·388	0·9998	None
1F	34·59	1·392	0·9999	
2B	54·02	2·521	0·9996	44·4
2F	54·09	2·509	0·9996	
3B	93·04	4·253	0·9989	42·7
3F	93·21	4·235	0·9989	
4B	149·0	6·500	0·9985	48·3
4F	149·0	6·491	0·9982	

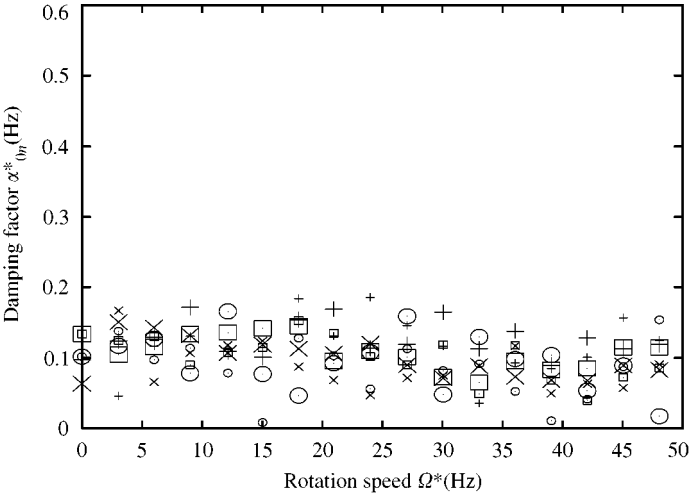

Figure 4. Damping factors at low pressure for BTWs (small points) and FTWs (large points) of: +, mode (0, 1); ×, mode (0, 2); □, mode (0, 3); ⊙, mode (0, 4).

show no significant dependency upon rotation speed or mode number, and the average is about 0·1 Hz for all modes.

The absence of distinct damping characteristics of the wave pairs indicates that the estimated damping factors are the results of structural damping only. FTWs and BTWs are equally damped, and a difference between the damping factor of a FTW and the corresponding BTW must therefore express a measurement error. Computing these differences for all modes and taking an average over the 17 measurements, the measurement error on the damping factors is estimated to be about 0·05 Hz, or 50% of the average.

4.2.2. At ambient pressure

The chamber is opened and the disk rotates at ambient atmospheric pressure. Wave frequencies and damping factors of the four wave pairs are estimated at 35 rotation speeds in the speed range 0–48 Hz at intervals of 1 or 2 Hz.

In Figure 5 the estimated natural frequencies of each wave are displayed versus rotation speed. Now the natural frequencies of the FTW and BTW seem to be slightly different: The difference increases with increasing rotation speed and exceeds the measurement error of $0{\cdot}1(1 + n)$ Hz.

The curve fits based on relation (15) still captures the dependence of the natural frequency on rotation speed. The results are listed in Table 2, together with estimated critical speeds. The slopes of the curves for the BTWs are 3–7% larger than those for the FTW which also indicates a splitting of the natural frequencies.

In Figure 6 the estimated damping factors of the FTWs and BTWs are displayed versus rotation speed. The estimated damping factors of the FTWs now become substantially larger than those of the BTWs at higher rotation speeds. The difference increases with increasing rotation speed. Note that the last two damping factors of the BTW of mode (0, 3) are set to zero which denotes that these particular estimations were faulty.

4.2.3. Estimation of aeroelastic parameters and flutter speed

Flutter does not occur at a well-defined rotation speed in experiments. Renshaw *et al.* (1994) therefore suggested to define the flutter speed as being the rotation speed where the peak of

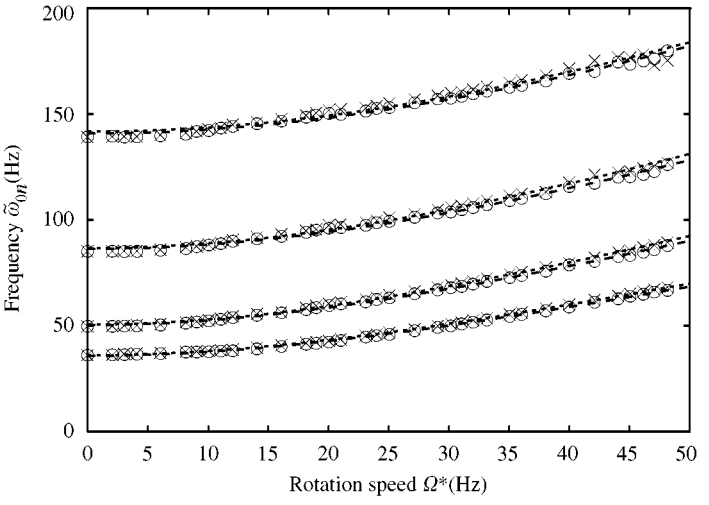

Figure 5. Natural frequencies calculated using relations (27): ×, based on wave frequencies of BTWs; ⊙, based on wave frequencies of FTWs; in both cases measured at ambient pressure. The curve fits are based on equation (16).

TABLE 2
Natural frequencies of the stationary disk ω_{0n}^{st*}, centrifugal stiffening coefficients s_{0n}, and critical speeds Ω_{0n}^{c*} at ambient pressure

Wave	ω_{0n}^{st*} (Hz)	s_{0n}	Correlation	Critical speed (Hz)
1B	36·10	1·435	0·9998	None
1F	35·83	1·362	0·9996	
2B	50·59	2·397	0·9990	39·9
2F	50·32	2·241	0·9991	
3B	86·74	3·886	0·9964	38·4
3F	86·36	3·608	0·9972	
4B	141·8	5·509	0·9854	43·8
4F	140·9	5·346	0·9955	

the critical wave is 20 dB above the noise level of the experimental frequency response. Based on this definition the flutter speed of the disk under the ambient conditions is about 55 Hz. The flutter mode is (0,3).

To predict this flutter speed and mode, the non-dimensional aeroelastic parameters c_{0n} and $c_{0n}\Omega'_{d_{0n}}$ of the four lowest asymmetrical modes are calculated from the damping factors (Figure 6) and the natural frequency of the BTWs using relations (27). The parameters are plotted as functions of a non-dimensional rotation speed in Figure 7. The non-dimensionalization is based on the natural frequency of mode (0, 1) of the stationary disk as characteristic time measure: $t_0 = (\omega_{01}^{st*})^{-1} \approx 0{\cdot}028$ s.

The damping coefficients c_{0n} seem to increase linearly with rotation speed, whereas the product of the damping coefficient and speed $c_{0n}\Omega'_{d_{0n}}$ shows a nonlinear trend. The curves in Figure 7 correspond to linear and second order polynomial fits to c_{0n} and $c_{0n}\Omega'_{d_{0n}}$, respectively,

$$c_{0n} \approx p_1 + p_2\Omega \quad \text{and} \quad c_{0n}\Omega'_{d_{0n}} \approx p_3\Omega + p_4\Omega^2 \tag{30}$$

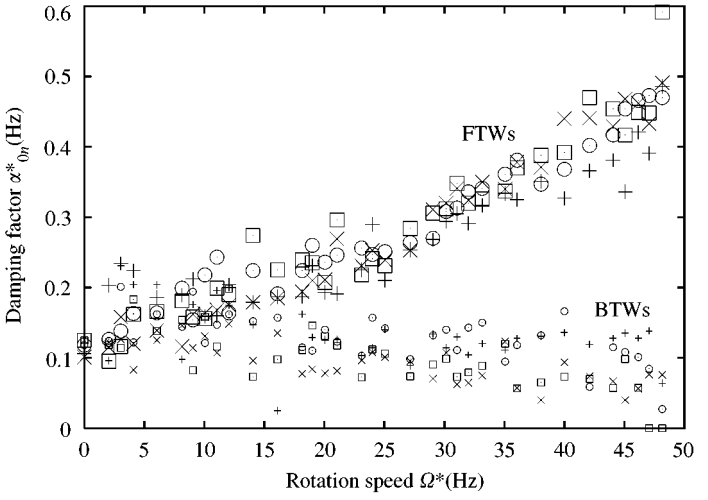

Figure 6. Damping factors at lambient pressure for BTWs (small points) and FTWs (large points) of: +, mode (0, 1); ×, mode (0, 2); □, mode (0, 3); ⊙, mode (0, 4).

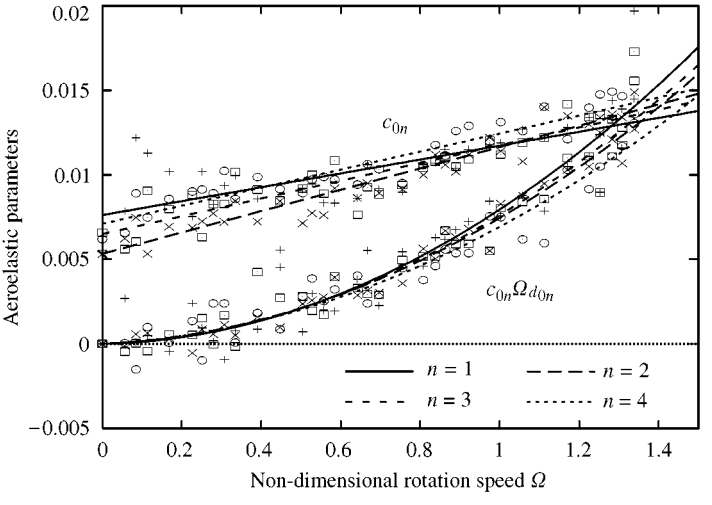

Figure 7. Nondimensional aeroelastic parameters c_{0n} and $c_{0n}\Omega'_{d_{0n}}$ computed from equation (28): +, mode (0, 1); ×, mode (0, 2); □, mode (0, 3); ⊙, mode (0, 4). The curve fits are based on equation (30).

The fitting parameters p_i are listed in Table 3. From these expressions (29), the damping speed in dimensional form can be estimated as

$$\Omega'_{d_{0n}}{}^* \approx \frac{p_3\Omega + p_4\Omega^2}{p_1 + p_2\Omega} t_0^{-1} \tag{31}$$

In Figure 8 the damping speeds of all four modes (30) are plotted together with the wave speeds $\tilde{\omega}^*_{0n}/n$ based on the previous curve fits of the natural frequencies to (15). By extrapolating the curves, we see that the first intersection of a wave speed curve and a corresponding damping speed curve occurs for the (0, 3) mode. This mode is identical to the observed flutter mode of the disk at ambient pressure. By solving $\Omega'_{d_{03}}{}^* = \tilde{\omega}^*_{03}/3$, we

TABLE 3
Parameters and correlation for fits to c_{0n} and $c_{0n}\Omega'_{d_{0n}}$ based on equation (30)

n	$p_1 \times 10^3$	$p_2 \times 10^3$	Correlation	$p_3 \times 10^3$	$p_4 \times 10^3$	Correlation
1	7·623	4·108	0·7413	0·4398	7·515	0·9393
2	5·326	6·318	0·9580	1·028	6·413	0·9867
3	6·501	5·255	0·9004	0·8292	6·782	0·9615
4	7·108	5·340	0·9367	1·178	5·745	0·9646

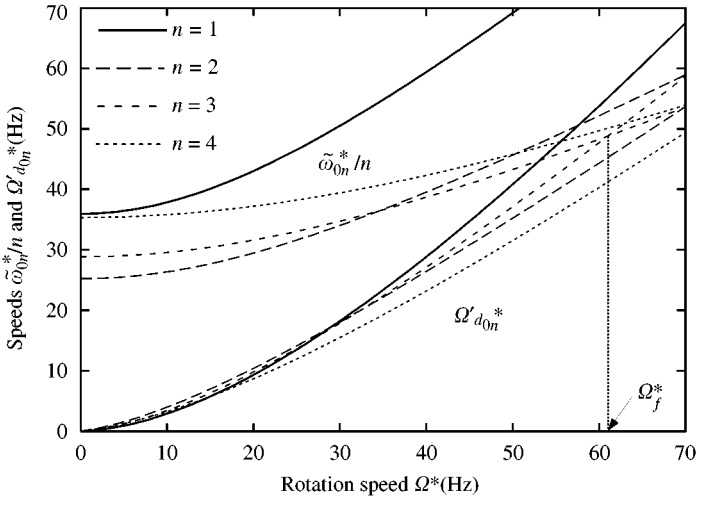

Figure 8. Wave speeds $\tilde{\omega}^*_{0n}/n$ (upper curves) and damping speeds $\Omega'^*_{d_{0n}}$ (lower curves).

predict the flutter speed $\Omega^*_f \approx 62$ Hz, which is about 13% higher than the observed flutter speed.

4.2.4. Summary and comparison of experiments

In both experiments, we obtain sufficient significance for the relationship between the natural frequencies and the rotation speed (16), arising from the centrifugal stiffening. This is illustrated in Figures 3 and 5 and shown by the correlation coefficients in Tables 1 and 2. However comparing the results of the curve fits in the two experiments, we make two observations: For all modes except mode (0, 1), the natural frequency decreases in the presence of surrounding air. Second, the relative differences between the slopes of the FTW and BTW versus rotation speed Ω is 3–7% at ambient pressure, but only about 0·5% in vacuum. This splitting of the natural frequencies in the presence of air, cannot be explained by measurement error.

When the disk is spinning in vacuum, no systematic difference in the damping characteristics for FTWs and BTWs was observed (Figure 4). Assuming that the wave pairs are equally damped by structural dissipation, the measurement error on the damping factors is estimated to be 0·05 Hz. Despite the large error on the damping factors, the effect of the aerodynamic loading on the damping of FTWs and BTWs is evident. The damping factors of the wave pairs in Figure 6 show clearly that FTWs are more highly damped than the BTWs due to the influence of the air. The difference between the damping factors increases

with rotation speed. As shown in Section 3, this observation can be explained by the representation of the aerodynamic pressure as a distributed rotating damping force. Using the relations in Section 3.2.1, we predict the flutter mode (0, 3) and the flutter speed within 13% of the observed speed.

5. DISCUSSION

In the presence of the surrounding air, we observe that the natural frequencies of all modes except mode (0, 1) decrease for values measured in the near absence of air. As a result, the critical speeds are decreased about 11% from those measured near vacuum. The effect of "added fluid mass", can explain the decrease for the higher modes, however it cannot explain why the natural frequency of mode (0, 1) is increased by the fluid loading. Another explanation is that the natural frequencies shifted due to a change of clamping conditions, which has a large influence on the frequencies (D'Angelo & Mote 1993*b*).

Similar to our results, Campbell (1924), D'Angelo & Mote (1993*b*) and others have showed that experimentally obtained natural frequencies depend on the rotation speed as described by the theoretical relation derived from the linearized Kirchhoff plate theory. However, the splitting of the natural frequencies of FTWs and BTWs due to the aerodynamic loading is not known to have been reported earlier. The slopes of the curve fits in Table 2 show that the estimated natural frequencies from the BTWs are larger than those from the FTWs. These slopes enclose the corresponding slopes of the natural frequencies in vacuum (Table 1). Thus, it seems that the airflow slows down FTWs but speeds up BTWs. This phenomenon might be explained by a distributed inertia force that rotates relative to the disk, thereby adding more apparent mass to FTWs than to BTWs (Hansen, 1999).

The error of 0·05 Hz on the damping factors has an important influence on the prediction of the flutter speed. One explanation of this error can be insufficient frequency resolution. A resonance peak in a FRF describing a damping factor of 0·1 Hz, has a 3 dB bandwidth of approximately 0·2 Hz (Ewins 1984). With a frequency resolution of 0·1 Hz, the upper 3 dB part of this peak is therefore described by two points (or fewer). Although a curve fitting procedure is used (SMS 1990), a higher resolution will improve the estimates of the damping factors. Another possible explanation for this error is rotation speed fluctuation due, for instance, to variations in laminar–turbulent flow transition on the disk. These fluctuations can have a large effect on the damping factors because the peaks of the FRFs are distorted through the direct dependence on the rotation speed (27). For example, if the speed variation is 0·01 Hz, the resonance peak in the FRF shifts $n \times 0{\cdot}01$ Hz. A flywheel or electronic speed control has been considered but not used to stabilize the rotation speed. Finally, a refinement of the experiment would be to measure the excitation force. This would improve the accuracy of the FRFs and thereby the damping factors.

Because of the error in the damping factors, the estimated structural damping factors cannot be directly compared to the damping factors of the waves under the influence of aerodynamic loading. Therefore, we cannot extract the effect of the structural damping from the estimated damping speeds $\Omega'_{d_{0n}}$ to obtain the actual damping speed defined by equation (5). This would require that the contribution of structural damping to the damping coefficient c_{0n} can be subtracted (cf. Section 2.3). Though, the presented results indicate that the actual damping speed is mode dependent and a nonlinear function of the rotation speed (cf. Figure 8), assuming that the structural damping is small compared to the aerodynamic damping. This observation differs from the modeling by (Yasuda et al. 1992) ($\Omega_d = \Omega C_L/C_D$), the modeling of a disk spinning in an unbounded inviscid fluid (piston theory with $\Omega_d = \Omega$), and the modeling of a disk spinning in a viscous fluid close to a wall (lubrication theory with $\Omega_d = \Omega/2$).

D'Angelo & Mote (1993*a*), who used the same set-up and disk, showed that the flutter speed increases inversely with decreasing fluid density. With the rotating damping model, this behavior can be explained by the decrease in the slope of the damping speed curves due to the decreased fluid density. Furthermore D'Angelo & Mote (1993*a*) showed that the flutter mode changed from mode (0, 3) to (0, 4) at a particular low pressure. The estimated wave speeds show that the speed of mode (0, 4) is less than the speed of mode (0, 3) above a transition rotation speed. Thus, this change in flutter mode can be explained by a sufficient decrease in density, where the slopes of the damping speed curves decrease such that the first intersection of a wave speed and a damping speed curve occurs for mode (0, 4). Additional experiments at low pressure will be important to support this understanding.

6. CONCLUSION

An experimental method for predicting flutter of a disk spinning in a fluid has been developed and illustrated by an experiment with a steel disk spinning in air. In the experiment, it is observed that the damping of forward traveling waves increases with the rotation speed, while the damping of backward traveling waves decreases. A reference experiment, performed on the disk in near vacuum, showed no systematic difference in the damping between these traveling wave pairs. These observations are explained by representing the aerodynamic pressure on the disk by a mode-dependent distributed viscous damping force that rotates relative to the disk. From experiments conducted in air, the speeds and magnitudes of the damping forces for the four lowest modes have been estimated at increasing rotation speeds. It is shown that the damping speeds increase nonlinearily with the rotation speed. By assuming that the trends of the damping speeds continue until flutter occurs, it was possible to predict the flutter speed and mode of the disk. The relative error in the prediction of the flutter speed was 13%. Refinements of the experimental set-up can likely improve the accuracy of the method.

REFERENCES

AHN, T. & MOTE, C. D. JR. 1998 Mode identification of a rotating disk. *Experimental Mechanics* **38,** 250–254.

CAMPBELL, W. 1924 The protection of steam-turbine disk wheels from axial vibration. *ASME Transactions* **46,** 31–160.

D'ANGELO, C. & MOTE, C. D. JR. 1993*a* Aerodynamically excited vibration and flutter of a thin disk rotating at superpercritical speed. *Journal of Sound and Vibration* **168,** 15–30.

D'ANGELO, C. & MOTE, C. D. JR. 1993*b* Natural frequencies of a thin disk, clamped by thick collars with friction at the contacting surfaces, spinning at high rotation speed. *Journal of Sound and Vibration* **168,** 1–14.

DOWELL, E. 1975 *Aeroelasticity of Plates and Shells*, 1st edition. Leyden: Noordhoff.

ELLIS, R. & MOTE, C. D. JR. 1979 A feedback vibration controller for circular saws. *ASME Journal of Dynamic Systems, Measurement, and Control* **101,** 44–49.

EWINS, D. 1984, *Modal Testing: Theory and Practice*, Letchworth, U.K.: Research Studies Press Ltd.

HANSEN, M. H. 1999, Aeroelasticity and dynamics of spinning disks, *PhD Thesis*, Technical University of Denmark, Department of Solid Mechanics, Lynghy, Denmark.

HOSAKA, H. & CRANDALL, S. 1992 Self-excited vibrations of a flexible disk rotating on an air film above a flat surface. *Acta Mechanica* **3,** 115–127.

HUANG, F. & MOTE, C. D. JR. 1995 On the instability mechanisms of a disk rotating close to a rigid surface. *Journal of Applied Mechanics* **62,** 764–771.

LEE, C.-W. & KIM, M.-E. 1995 Seperation and identification of travelling wave modes in rotating disk via diarectional spectral analysis. *Journal of Sound and Vibration* **187,** 851–864.

RENSHAW, A. 1998. Critical speed for floppy disks. *Journal of Applied Mechanics* **65,** 116–120.

RENSHAW, A. & MOTE, C. D. JR. 1992 Absence of one nodal diameter critical speed modes in an axisymmetric rotating disk. *Journal of Applied Mechanics* **59,** 687–688.

RENSHAW, A., D' ANGELO, C. & MOTE, C. D. JR. 1994 Aerodynamically excited vibration of a rotating disk. *Journal of Sound and Vibration* **177,** 577–590.

SMS 1990 *STAR* 2.00—*Reference and Applications.* Milpitas, California: Structural Measurement Systems.

TOBIAS, S. A. & ARNOLD, R. N. 1957 The influence of dynamical imperfection on the vibration of rotating disks. *Proceedings of the Institution of Mechanical Engineers* **171,** 691–703.

YASUDA, K., TORII, T. & SHIMIZU, T. 1992 Self-excited oscillations of a circular disk rotating in air. *JSME International Journal* **35,** 347–352.